Electrochimica Acta 485 (2024) 144035

Contents lists available at ScienceDirect

Electrochimica Acta

journal homepage: www.journals.elsevier.com/electrochimica-acta

A closed bipolar electrochemical cell for the interrogation of BDD single particles: Electrochemical advanced oxidation

Anna Dettlaff [a,1], Joshua J. Tully [b,1], Georgia Wood [b], Deep Chauhan [b], Ben G. Breeze [c], Lijiang Song [b], Julie V. Macpherson [b,*]

[a] Department of Chemistry, Gdańsk University of Technology, 11/12 Gabriela Narutowicza Street, Gdańsk 80-233, Poland
[b] Department of Chemistry, University of Warwick, Coventry CV4 7AL, UK
[c] Spectroscopy Research Technology Platform, University of Warwick, Coventry CV4 7AL, UK

ARTICLE INFO

Keywords:
Boron doped diamond (BDD)
Single particle
Bipolar electrochemistry
Closed bipolar cell
3D printed cells
Electrochemical advanced oxidation
Electrochemical oxidative removal
HPLC-MS
Dyes
Methylene blue

ABSTRACT

A closed bipolar electrochemical cell containing two conductive boron-doped diamond (BDD) particles of size ~ 250 – 350 μm, produced by high-pressure high-temperature (HPHT) synthesis, has been used to demonstrate the applicability of single BDD particles for electrochemical oxidative degradation of the dye, methylene blue (MB). The cell is fabricated using stereolithography 3D printing and the BDD particles are located at either end of a solution excluded central channel. Platinum wire electrodes placed in each of the two outer solution compartments are used to drive electrochemical reactions at the two BDD particles, which, under bipolar conditions do not require direct electrical connection to a potential source. Experiments using ultra high-performance liquid chromatography coupled with mass spectrometry (UHPLC-MS) show that the anodic pole BDD particle is able to electrochemically remove > 99 % of the dye (originally present at 1×10^{-4} M) to undetectable UHPLC-MS products in 600 s. Monitoring of the time dependant change in MB peak area, from the UHPLC chromatograms, enables a pseudo first order rate constant of 0.54 min^{-1} to be determined for MB removal. Given the large scale at which such particles can be produced (tonnes), such data bodes well for scale up opportunities using HPHT-grown BDD particles, where the particles can be assembled into high surface area electrode formats.

1. Introduction

Synthetic boron-doped diamond (BDD) has attracted much attention in the electrochemical community due to its remarkable properties such as low background currents, high overpotential for oxygen and hydrogen evolution in aqueous electrolytes, high chemical inertness in aggressive media, *etc*. [1–3]. BDD is typically grown using chemical vapour deposition (CVD) [2], due to the ability to incorporate high levels of uncompensated boron into the diamond lattice such that metal-like conductivity is achieved. However, CVD suffers from relatively slow growth rates and poor scalability. High-pressure high--temperature (HPHT) synthesis in contrast can produce significantly larger volumes, at the tonnes scale if required, of micron to sub-mm sized particles, with faster growth rates compared to CVD, and at a lower cost. The main issue with using HPHT for the synthesis of metal-like BDD is the difficulty of preventing nitrogen incorporation from the atmosphere. Any nitrogen incorporated into the lattice will pair with boron (compensation) resulting in a decrease in the charge carrier concentration [4]. Recently, it has been shown that aluminium diboride (AlB_2) can be used as both a boron source and as an agent to remove nitrogen during the HPHT growth process. This process results in the growth of BDD particles, as small as 80 μm in size and doped with enough boron > 10^{20} B atoms cm^{-3} [5] to demonstrate metal-like electrochemical behaviour [6,7].

For many industrial electrochemical applications, large surface area electrodes are desirable. One such application is electrochemical oxidative degradation [8] of pollutants in water systems, where the electrochemical generation of highly oxidising species or electrochemical oxidation of the pollutant itself leads to degradative removal of the pollutant from solution [9]. BDD has proved particularly popular as an electrode in oxidative degradation due to its high stability and ability to generate very high oxidative potential, hydroxyl radicals from water oxidation [1,10]. Areas of current activity involve the use of BDD electrochemical oxidative degradation approaches for the removal of *e.g.*

* Corresponding author.
E-mail address: j.macpherson@warwick.ac.uk (J.V. Macpherson).
[1] These authors contributed equally to this work.

https://doi.org/10.1016/j.electacta.2024.144035
Received 21 December 2023; Received in revised form 6 February 2024; Accepted 28 February 2024
Available online 29 February 2024

pharmaceuticals [10], perfluoroalkyl and polyfluoroalkyl substances [11] and dyes [12,13]. However, for all these applications the BDD is employed in a planar electrode format, grown via CVD. In contrast, BDD particles arranged in three dimensional architectures offer a route for the formation of high surface area (porous) electrodes [14].

Before scaling up it is useful to validate the electrochemical behaviour of a single particle for the application of interest, here electrochemical oxidative degradation. Previous approaches to single particle electrochemical measurements have employed masking procedures [6] and/or micropositioning [15] methods in order to position and electrically contact the particle. Alternatively, high resolution electrochemical imaging techniques have been used to electrochemically interrogate isolated BDD particles sitting on a conducting support [16]. However, these approaches are fairly complex and/or require specialist equipment to make electrical contact to the particle. To overcome this, we describe the use of a bipolar electrode (BPE) set-up.

In bipolar electrochemistry, the cell is typically operated in open mode, where a potential difference is applied between two outer electrodes under resistive solution conditions, such that a uniform electric field is applied across the electrolyte solution [17]. By placing a conductive object in this field, the object experiences an interfacial potential difference across its length without being directly connected to the potential source. In the case of a particle placed within the field, increasing the diameter of the particle increases the interfacial potential difference experienced either side of the particle. Given the particle sizes used in this paper (250 – 350 μm) unfeasibly large potentials would need to be applied in order for sufficient interfacial potential differences to be established across a single particle in order to drive the oxidative degradation processes.

To overcome this limitation, we adopt a closed BPE cell arrangement [18–20], Fig. 1 (top), which contains two BDD particles, which constitute the two poles (anodic and cathodic) of the bipolar electrode cell. Each pole is separated by a length of electrically conductive silver epoxy which is electrically isolated from solution. Each end of the silver epoxy is connected to an individual BDD particle sitting in the anodic or cathodic pole solution compartment. In this way the closed BPE cell is analogous to two series coupled electrochemical cells, as has been demonstrated for both macro- [21] and microelectrodes [19]. The closed BPE cell can be electrically considered as five resistances (*R*) in series, as shown schematically in Fig. 1 (bottom). They include, two solution resistances, R_{sol}, in the two solution compartments, the resistances associated with the BPE, R_{BPE} [17] and charge transfer, R_{ct}, at the surface of the two BDD particle electrodes. Closed bipolar electrode arrangements have been previously used as *e.g.* electrochromic detectors for chemical sensing in aqueous and non-aqueous solutions [22] and more complex media such as blood [23], leakless reference electrodes [24,25] and substitutional stripping voltammetry [26].

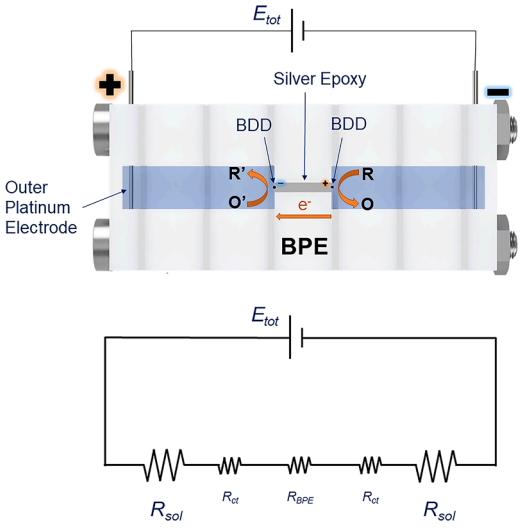

Fig. 1. (Top) Schematic of the closed BPE set-up for the two BDD particle electrodes. The current passed due to reduction of O' to R' at the cathodic pole particle (-ve) equals that passed at the anodic pole particle (+ve) due to oxidation of R to O. (Bottom) The closed BPE cell as expressed in terms of the resistances, R_{sol}, R_{BPE} and R_{ct}.

In the closed BPE arrangement the potential is applied to the two platinum outer electrodes and the reverse polarities are seen on the two BDD particles [17]. Application of this driving potential results in equal but opposite faradaic currents being passed at the two BDD particles [19]. Hence, in accordance with Fig. 1 (top), the BDD particle on the left-hand side is biased negatively (cathodic pole) and promotes reduction of species O' to R', whilst the BDD particle on the right-hand side is biased positively (anodic pole) and promotes oxidation of R to O. In the case where the two particles are unequal in size and / or exposed to different analyte concentrations / unequal diffusion coefficients of analytes, the side of the closed BPE arrangement where the smallest current is passed controls the current flow through the system. In this paper, we investigate the capabilities of a single BDD particle, functioning as the anodic pole in a closed BPE cell, towards electrochemical oxidative degradation of the dye molecule, methylene blue.

2. Experimental

2.1. Chemicals and solutions

All solutions were prepared using ultrapure deionised water (≥ 18.2 MΩ cm, Milli-Q, Millipore Corp., USA). All chemicals were used as received and include potassium nitrate (KNO_3; ≥ 99.0 %; Merck) and methylene blue chloride (MB^+Cl^- = 3,7-bis(dimethylamino)phenothiazin-5-ium chloride, CAS 61–73–4, dye content 94.0 %; Merck). Ferrocene tetramethylammonium ($FcTMA^{+/2+}$) hexafluorophosphate was produced via the metathesis of the corresponding iodide salt (99 %, Strem) with ammonium hexafluorophosphate (99.5 %, Strem). Potassium ferri-(III)-cyanide ($K_3[Fe(CN)_6]$, 99 %, Sigma-Aldrich) was used as received. For the BPE pH experiments, universal indicator dye (Scientific Laboratory Supplies; pH 4 – 11, 1 wt% in ultrapure water) was employed. Solution conductivity and pH were measured using an InLab 738-ISM-5 m conductivity probe, and InLab Expert Go-5m-ISM pH Probe (Mettler Toledo SevenGo Duo pH/conductivity meter).

2.2. BDD particle preparation

The BDD particles were prepared using HPHT synthesis, as described in reference [6], using AlB_2 as the source of boron. 5 g of graphite powder (S9, Morgan Advance Materials, 50 wt%), 3.5 g of iron powder (Fe > 99.5 CIP CN, BASF, 35 wt%), 1.5 g of nickel powder (Ni > 99.85%, type 123, Vale, 15 wt%), and 0.002 g of diamond seed (US Mesh 100 diamond seed, 1.60 – 1.77 μm diameter, polycrystalline diamond micron grade 2, Element Six Ltd), were mixed with a turbulent mixer for 30 mins, in the presence of a single steel ball, 10 mm in diameter. 1.525 g of this mixed powder was then added to 500 g of graphite (50 wt%), 350 g of iron (35 wt%) and 150 g of nickel (15 wt%), and mixed further using a cone blender for 3 h, facilitated by the addition of 200 g of the same steel balls, added in a mass ratio of 1:5 (steel balls: powder). The resulting powder was combined with 4.8 wt% of AlB_2 and mixed for 1 h using the cone blender with the steel balls added at the same ratio as above. This wt% of AlB_2 was sufficiently high to enable the synthesis of BDD with a B atom density of $>10^{20}$ atoms per cm^3, which is necessary to achieve metal-like conductivity [5]. The resulting boron containing powders were then sieved to remove the balls, compacted into cylinders and heated to 1050 °C under vacuum to remove oxygen and hydrogen impurities. Synthesis was then carried out at 5.5 GPa and 1300 °C in a cubic anvil HPHT apparatus.

To eliminate any remaining metals, unreacted graphite, and other

forms of sp^2 bonded carbon that may have formed on the surface of the BDD, a series of stringent cleaning treatments using hydrochloric acid, sulphuric acid and nitric acid mixtures and water ultrasonication was implemented, see reference [6] for further details. Following the cleaning procedures, the BDD particles were left to dry overnight in an oven at a temperature of 60 °C. The particles were then sieved using a woven wire mesh sieve (Retsch, Germany) to separate out the particles larger than 250 μm in diameter. Particles with diameters > 250 – 350 μm were selected for this work for ease of handling and were predominantly polycrystalline in texture.

2.3. BPE cell

The closed BPE cell was designed in Fusion 360 (Autodesk, USA) and printed on a Form 3 (FormLabs, USA) stereolithography 3D printer using polymethylmethacrylate (PMMA) resin (Standard Clear, FormLabs, USA) [27]. The design consisted of three distinct parts; (1) an outer electrode compartment containing two platinum wires (length 4.5 mm, diameter 0.75 mm) at a separation distance of 40 mm, (2) a channel section (1.00 × 9.70 × 0.75 mm) situated in the centre of the cell, which was filled with conductive silver epoxy (CircuitWorks, Chemtronics, USA) and housed two BDD particles, one at each end, with the top surface of the channel coated in an insulating resin (Clear, FormLabs) and (3) two separate solution compartments (of volume 210 μL) each in contact with a BDD particle. The overall cell was of dimensions 17.0 (w) × 66.0 (l) × 5.5 (h) mm. For some experiments, where the electrolysis products associated with processes occurring on the platinum outer electrodes were a possible concern, a Nafion membrane (Nafion® 424 reinforced with poly(tetrafluoro-ethylene fibre, 0.33 mm in thickness, Sigma-Aldrich) was used. This reduced the volume of solution each BDD particle was exposed to, to 170 μL.

Placement of the HPHT grown BDD particles at either end of the channel section was relatively easy and involved positioning the closed BPE cell under a microscope (with 5 × magnification) to aid the BDD particle manipulation process. Tweezers were used to pick up and place the BDD particles in their appropriate locations. Once positioned, the area around the BDD particle was flooded with the same insulating resin as used to insulate the silver epoxy filled channel, leaving the top surface of each particle exposed. A 3D rendering and photograph of the closed BPE cell is shown in Fig. 2a and b, respectively. The BDD particles are referred to as BDD-1 (cathodic pole) and BDD-2 (anodic pole; see Fig. 2a). Optical images of the BDD HPHT particles used in this work are also shown in Fig. 2a. Fig. S1a shows a higher resolution, field emission scanning electron microscope (Zeiss Gemini) image of a BDD particle. The cell was assembled using two M3 bolts. The platinum outer electrodes were connected to a benchtop DC power supply (VLP-2602 OVP, Voltcraft) and the desired driving potential (E_{tot}) applied. Due to the ease of preparation, four cells were prepared for evaluation.

2.4. Raman

Raman spectroscopy measurements were collected using a Horiba LabRam HR Evolution spectrometer with a 488 nm laser (nominally 40 mW) and 600 l/mm grating, at 25 % laser power (nominally 10 mW), using a × 50 LWD 0.6 numerical aperture objective.

2.5. Electrochemistry

Voltammetry of the BDD particles was carried out in the closed cell configuration using an AUTOLAB PGSTA302N (Autolab, Metrohm, Switzerland) potentiostat–galvanostat with Nova 2.1.2 software. All electrochemical experiments were conducted in a two-electrode configuration by driving a potential difference between the two outer platinum electrodes in the closed BPE cell. For electrochemical characterisation of the BDD particle electrodes, the anodic channel compartment contained 1 mM $FcTMA^+$ in 0.1 M KNO_3 and the cathodic compartment, 5 mM $[Fe(CN)_6]^{3-}$ also in 0.1 M KNO_3. For water splitting experiments, universal indicator dye was added to the ultrapure water in both solution compartments, whilst for the methylene blue experiments, a solution of 1×10^{-4} M MB^+ was employed.

2.6. Ultra high performance liquid chromatography–mass spectrometry (UHPLC-MS) and gas chromatography-mass spectrometry (GC-MS)

UHPLC-MS analysis was carried out to determine the electrochemical products in the anodic and cathodic pole solutions of the BPE set-up when using aqueous starting solutions containing 1×10^{-4} M MB in both solution compartments. 30 μL samples were taken from the anodic pole solution after 0, 30, 120, 300, 600, and 900 s of BPE electrolysis and from the cathodic pole solution after 0, 600, and 900 s of BPE electrolysis. Moreover, additional electrolysis and products analyses were conducted for a highly concentrated solution of MB^+ (0.1 M MB^+) after 2400 s (40 min) of electrooxidation. UHPLC-MS analysis was performed with a Dionex 3000RS ultra high performance UHPLC coupled to a Bruker MaXis II Q-TOF MS. An ACE Ultracore Super C18 column (C18, 150 × 2.1 mm, 2.5 μm) with a guard column (C18, 10 ×

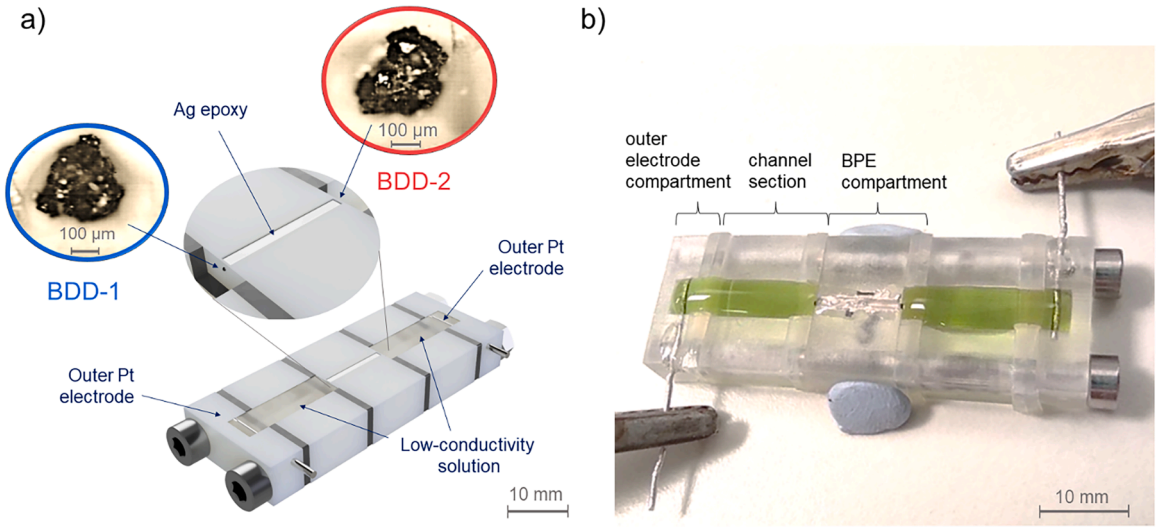

Fig. 2. BPE closed configuration cell containing two BDD particles at either end of the channel section, BDD-1 (cathodic pole) and BDD-2 (anodic pole), (a) schematic with optical images of typical BDD particles also shown and (b) an optical image of the 3D printed cell.

2.1 mm) was used with the column temperature at 30 °C. Mobile phases consisted of A (water with 0.1 % formic acid) and B (acetonitrile with 0.1 % formic acid). After 5 min of an isocratic run at 5 % B, a gradient of 5% B to 100 % B in 25 min was employed with a flow rate at 0.2 ml / min. The MS was operated in electrospray positive mode with a scan range 50 - 2500 *m/z*. Source conditions were: end plate offset at −500 V; capillary at −4000 V; nebulizer gas (N_2) at 1.8 bar; dry gas (N_2) at 8 L min^{-1}; dry temperature at 210 °C. Ion transfer conditions were: ion funnel 1 RF at 200 Vpp; multipole RF at 100 Vpp; quadruple ion energy at 4 eV, quadrupole low mass set at 50 *m/z*; collision energy at 7.0 eV; collision RF ramping from 550 to 2000 Vpp; transfer time set from 60 to 155 μs; pre-pulse storage time set at 5 μs. Calibration was performed with sodium formate (1×10^{-2} M) through a loop injection of 10 μL of standard solution at the beginning of each run.

Gas chromatography coupled with mass spectrometry (GC–MS) analysis was conducted with an Agilent 5977B and an Agilent DB5 column (30 m × 0.25 mm × 0.25 μm). 170 μL of solution from the anodic pole compartment was taken after 900 s of electrooxidation. Before measurements, the solution was extracted with an equal volume of dichloromethane (twice), then combined and dried with anhydrous sodium sulphate. 1 μL was injected into the GC–MS at 275 °C in splitless mode. The MS was operated with an EI source and a mass scan range 50 – 750 *m/z*.

3. Results and discussion

Prior to cell construction, individual BDD particles were characterised by Raman spectroscopy to verify the particles were suitably doped for electrochemical measurements and to assess their material properties. Five particles were chosen at random from the > 250 μm diameter sieved particles, with all five showing similar Raman signatures; a typical Raman spectrum over the wavenumber range 500 – 2000 cm^{-1}, is shown in Fig. 3a. All the spectra showed a diamond Raman line at 1328.5 ± 0.2 cm^{-1}, which was slightly red-shifted compared to that for intrinsic diamond (1332.0 - 1332.5 cm^{-1}) [6,28]. This is due to a tensile residual stress in the diamond lattice caused by the presence of boron [28,29]. The asymmetric Fano resonance (indicative of sufficient boron doping for the particle to exhibit metal-like conductivity [30]) is clearly visible, demonstrating that the BDD particles are doped above the metallic threshold [6]. There is no evidence of a peak associated with sp^2 carbon at ~ 1580 cm^{-1} [31], indicating that the particles are phase pure. Raman spectra for the other four particles can be found in SI 1 (Fig. S1b).

Electrochemical characterisation of the BDD particles was performed in the closed BPE set-up using cyclic voltammetry (CV), where the potential was applied between the two Pt outer electrodes. One compartment (anodic pole) contained a solution of 1 mM $FcTMA^+$ in 0.1 M KNO_3 and the other (cathodic pole) a solution of 5 mM $[Fe(CN)_6]^{3-}$ in 0.1 M KNO_3. The CV response was recorded at 0.1 V s^{-1}, scanning first in an oxidative direction, as shown in Fig. 3b. The five times excess of $[Fe(CN)_6]^{3-}$ added to the cathode compartment should be sufficient to ensure the CV is current limited by the $FcTMA^{+/2+}$ redox process [18]. The response, where the CV shows small peaks on the forward and reverse scan directions is indicative of mixed mass transport behaviour *i.e.,* where the response is neither dominated by linear or radial diffusion. This is expected given the size of the polycrystalline particles used in this study (250 – 350 μm effective geometric diameter) and means it is not possible to ascertain the exposed electrode area using analytical electrochemical expressions. This is further complicated by the inherent surface roughness of the polycrystalline BDD particles, as shown in Fig. S1a.

Before performing a closed cell BPE electrochemical oxidative degradation experiment, the ability of the two BDD particles to electrochemically oxidise / reduce water using the BPE set-up was explored. Electrochemical oxidation / reduction of water will result in a local decrease / increase in pH, respectively [32]. Here, electrochemical water splitting by BDD-1 (cathodic pole) and BDD-2 (anodic pole) was

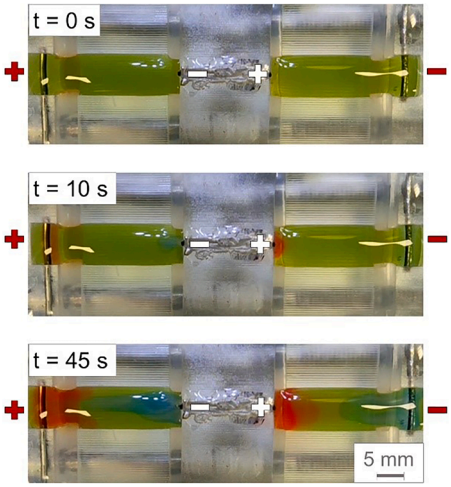

Fig. 4. Optical images of the BDD-BPE set-up as a function of time, t = 0, 10, and 45 s for electrochemical water splitting recorded in ultrapure water and universal pH indicator ($E = \pm$ 25 V).

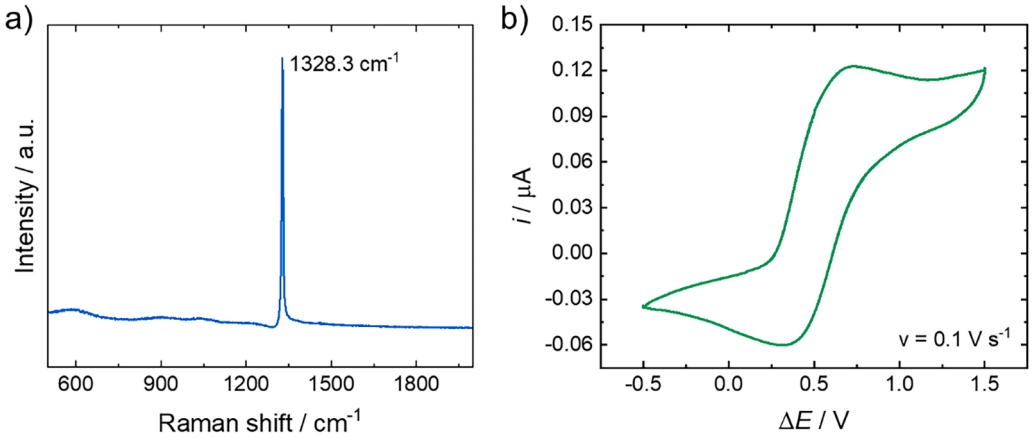

Fig. 3. Typical (a) Raman spectra of *a* > 250 – 350 μm diameter BDD particle, recorded with a 488 nm laser. (b) CV response of a BDD particle recorded using the closed BPE cell (second scan), with one channel compartment containing 1 mM $FcTMA^+$ in 0.1 M KNO_3 and the other 5 mM $[Fe(CN)_6]^{3-}$ in 0.1 M KNO_3, at a scan rate of 0.1 V s^{-1}.

assessed indirectly by monitoring the change in local pH via a solution colour change, in the presence of universal indicator (pH 4 – 11). Fig. 4 shows the time, *t*, dependant colour changes of the indicator for $t = 0$ s (top), = 10 s (middle), = 45 s (bottom) upon application of a potential difference of ± 25 V (E_{tot} = 50 V) between the two outer platinum electrodes; the left-hand platinum electrode is positive whilst the right-hand platinum electrode is negative. A video of the water splitting reaction on the two BDD particle electrodes in the BPE set-up is also available as video download 1.

Unlike the electrochemical characterisation experiment in Fig. 3b, here only ultrapure water is used in the solution compartments (in the presence of the pH indicator). The resistivity, ρ, of the solution = 46.1 kΩ cm and using $R_{sol} = \rho\, l / A$, where *l* and *A* are the length and area of the solution compartment = 1.300 cm and 0.450 × 0.215 cm respectively, R_{sol} = 620 kΩ. In contrast, R_{sol} = 1.0 kΩ for the experiments in Fig. 3b (for ρ = 78.1 Ω cm in 1 mM $FcTMA^+$ and 0.1 M KNO_3). The estimated resistance of the BPE, R_{BPE}, is *ca.* 70 Ω (estimation calculations are presented in SI 2, but do not include contact resistance between the BDD particle and silver epoxy). R_{ct} is expected to be of a similar magnitude (or smaller) to R_{BPE} based on impedance measurements made at BDD electrodes grown using CVD methods [33]. Thus in these experiments (Fig. 4), R_{sol} is the dominating resistance and a significant potential is dropped across the highly resistive solutions in both compartments when driving current through the BPE. Much higher potentials are now required than would be envisaged based on thermodynamic considerations alone [34,35], to produce sufficient concentrations of protons and hydroxide ions at the BDD poles to record noticeable solution colour changes.

At $t = 0$ s, in each compartment, the solution is green and reflective of the starting pH of the solution (pH ~ 7). At $t = 10$ s, the solution local to BDD-1 (cathodic pole) has turned blue indicative of a pH change from 7 to 9 (extending *ca.* 2.7 mm from the particle), due to the reduction of water to hydroxide ions. In the vicinity of BDD-2 (anodic pole), the solution has turned red (extending *ca.* 1.4 mm from the particle) and is indicative of a pH change from 7 to ≤ 4 due to the positively biased particle oxidising water to produce protons. With increased time, the colour change profile has extended further away from both BDD single particle electrodes and there is now an obvious reverse colour change at the two platinum electrodes [17]. Note, the current flowing in this experiment was below the current resolution (mA) of the power supply used, and thus could not be measured.

The behaviour of the BDD single particle BPE electrode towards electrochemical oxidative degradation of the dye molecule, MB^+Cl^- was next investigated [36]. In electrochemical degradation analysis a variety of techniques are used which can either monitor removal of the pollutant of interest, measure formation of reaction intermediates or quantify the extent of the degradation process. These include chemical oxygen demand (COD), total organic carbon (TOC) [37], spectrophotometric techniques (UV–Vis spectroscopy, fluorescence spectroscopy) [38,39] and liquid or gas chromatography with a suitable detector [38]. In this investigation, we chose to use UHPLC-MS as the main analysis technique. This is due to: (1) MB^+ can be easily detected using MS with UHPLC enhancing the detection sensitivity; (2) UHPLC-MS can inform on MS-detectable intermediates arising from electro-oxidation (and electro-reduction) of MB^+ in the BPE set-up, with the exception of products which are poorly ionised (often due to being hydrophobic or highly volatile); (3) TOC and COD methods require much larger volumes of solution than is available here and hence precludes their use; the volume of solution in the BDD particle anode compartment is only 170 μL. For these experiments, no excess supporting electrolyte was added to remove consideration of electrolysis of electrolyte anions and to simplify sample preparation for UHPLC-MS measurements. This study represents the first time HPHT grown BDD particles have been assessed for any electrochemical oxidative degradation application. For MB^+ removal, previously thin film CVD grown BDD electrodes, of diameter 10 cm were used to electrochemically degrade MB^+ [40] employing a single compartment electrochemical flow cell.

Electrochemical degradation of MB^+ was carried out using the BDD BPE single particle electrodes with ± 30 V applied between the two outer platinum electrodes. A solution of 1×10^{-4} M MB^+ (ρ = 54.6 kΩ cm^{-1}, R_{sol} = 733 kΩ, pH = 7.27 ± 0.01) was pipetted into each of the two BPE channels. A Nafion membrane was added between the outer electrode compartments and solution channels, to prevent any possible (large) ionic products of MB^+ electrolysis at the platinum outer electrodes moving into the solution compartments associated with the two BDD particle electrodes. Fig. 5 shows the colour changes associated with the BPE anodic pole oxidative processes over a period of 900 s. The corresponding video (at × 10 speed) is available as video download 2. After 120 s, the solution in the anodic pole compartment has become significantly paler in colour, and completely de-colourises after 600 s. Similar behaviour was seen for MB^+ degradation in three other BPE cells (as shown in Fig. S3, SI 3). In contrast, the cathodic pole solution over 900 s does not appear to change colour significantly (Fig. S4, SI 3). It is interesting to observe that the solution exposed to the platinum wire anode (diameter 0.75 mm and immersed fully in the solution compartment) does not fully decolourise after 900 s (Fig. S4 and video download 2), even though the electrode is significantly larger than the BDD particle. This further highlights the ability of BDD electrodes to produce species such as highly oxidising hydroxyl radicals from water oxidation, which can aid breakdown of MB^+. We also note changes in solution pH, due to water splitting at the two BDD electrodes (Fig. 4), do not cause a change in the extinction coefficient of MB^+, as verified using UV/Vis spectroscopy for MB^+ in pH solutions 2 to 9.

In order to provide further information about the chemical composition of the solutions, chemical analysis as a function of BPE electrolysis time (for the anodic pole solution: $t = 0$, 30, 120, 300, 600 and 900 s, for the cathodic pole solution: $t = 0$, 600 and 900 s) was carried out using UHPLC-MS. Each time point was run as a separate experiment, with a fresh solution used each time. Products of the electrolysis were identified using the MS in full SCAN mode in the mass range 50 – 2500 *m/z*. The resulting UHPLC-MS chromatograms are presented in SI4, Fig. S5. For all data, UHPLC-MS revealed only one peak which based on the mass-charge values (*m/z*), was assigned to MB^+ (*m/z* = 284, 3,7-bis (dimethylamino)phenothiazin-5-ium ion) (Fig. S6, SI 4) [41].

In the anodic pole solution, for all times ≥ shortest sampling time = 30 s, no intermediates of MB^+ degradation, such as 2,5-diaminobenzenesulfonic acid and 4-aminocatechol, as theoretically postulated by Teng *et al.* [42], were detected using UHPLC-MS. Although the sensitivity of the UHPLC-MS technique is usually in the range of 0.001 – 1 μg/L (dependent on the compound), we cannot rule out intermediates being present but at concentrations below the detection limit. An additional experiment was performed where the starting solution of MB^+ in a BPE cell was increased 1000-fold to 0.1 M and electrolysis in the small volume cell carried out for 2400 s. However, even under these more concentrated and extended time conditions, no intermediates could be detected, as seen in the chromatograms in Fig. S7, SI 4. GC–MS was also employed in order to look for possible intermediates not detectable using UHPLC-MS, such as lower molecular weight compounds of MB^+ degradation, or more volatile species *e.g.*, benzothiazole [42]. The experiments were performed on a 1×10^{-4} M MB^+ solution after anodic electrolysis for 900 s. Again, no by-product compound could be detected. The data above also suggests that if there are intermediate species they are not in a form to be detectable by UHPLC or GC–MS or the electrochemical breakdown pathway of MB^+ to the final products (CO_2 and H_2O) is faster than the timescale of solution sampling.

The area under the MB^+ peak, visible in the UHPLC-MS chromatograms at the retention time of *ca.* 15.5 min (Fig. S5, SI 4), was thus used as a quantitative guide to the rate of MB^+ removal as a function of time, as shown in Fig. 5. UHPLC-MS shows that the area associated with the MB^+ peak decreases with time from 100 % (0 s), to 82.9 % (30 s), 41.0 % (120 s), 5.8 % (300 s) and 0.6 % (600 s), with no evidence of any MB^+ remaining in the solution at 900 s. Assuming pseudo first order kinetic

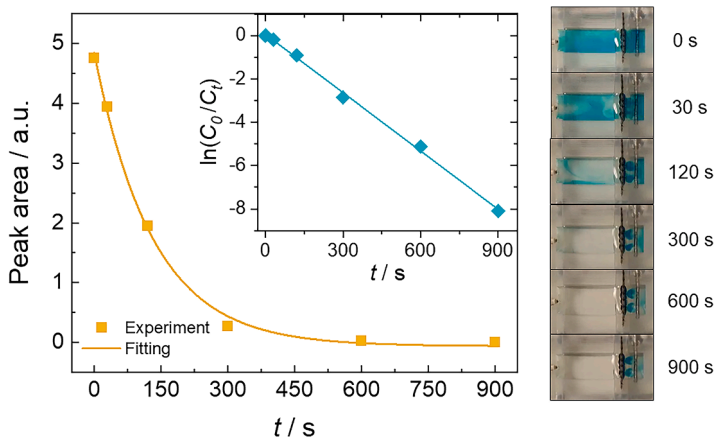

Fig. 5. Left image: change in peak area for MB^+, from UHPLC-MS chromatograms, recorded as a function of time ($t = 0 – 900$ s) in the anodic pole solution ($E = \pm 30$ V). Right image: optical images of the anodic pole solution compartment as a function of time during the MB^+ electrochemical oxidation process. Note, the BDD particle is visible as the small black dot at the left hand side of the image. Inset, a pseudo-first order kinetic plot for MB^+ degradation.

removal of MB^+ [42], the area under the peak, which equates to MB^+ concentration, was used to extract a rate constant (k) for the electrochemical removal of MB^+. The inset to Fig 5 shows a plot of $\ln(C_0/C_t)$ *versus* time, where C_0 is the area under the MB^+ peak at time = 0 s and C_t the area under the peak at time, t. The gradient gives a value for k of 0.54 min^{-1} ($R^2 = 0.998$), which interestingly is very similar to the values reported in reference [42] (0.46 – 0.57 min^{-1} for pH values 11 – 3) for MB^+ removal using an electro-Fenton method and significantly larger electrodes (0.6 × 12 cm).

In the cathodic pole solution, at $t = 0$ s, the blue colour is homogeneous (SI3, Fig. S4), after 120 s the blue colour has slightly intensified in the centre of the compartment, with lighter / colourless regions around the edge. After 900 s of BPE electrolysis, there is a small decrease in the peak area of the MB^+ signal compared to the starting solution at $t = 0$ s (Fig. S4, right hand side, SI 3). Whilst MB^+ can be electrochemically reduced to leucomethylene blue, SI 5, Fig. S8–9 [43], which is colourless, there is no evidence of its formation at the detection levels offered by UHPLC-MS (Fig. S5–6, SI 4). The origin of this colour inhomogeneity is interesting. In this set-up no supporting electrolyte is added to the solution and there will be significant potential field effects. Movement of species by migration, where MB^+ will preferentially move towards the cathodic pole BDD electrode is thus expected. Video download 2 also shows significant solution convection in both compartments. Interestingly, when supporting electrolyte (0.1 M KNO_3) is added to the MB^+ solution, solution convective effects are significantly minimised and the solution in the cathodic compartment now remains uniformly coloured throughout the electrolysis process (video download 3). Hence the observed solution convection is strongly linked with potential field effects [44].

4. Conclusions

We have demonstrated, through the use of a simple closed configuration BPE cell, a method for interrogating the electrochemical activity of single particles, without the need for a direct electrical connection to the particle. In particular we have used the closed BPE set-up to investigate the effectiveness of a single polycrystalline BDD particle (250 – 350 μm in size) for the degradative electrochemical oxidation of the dye MB^+. Given the small sample volumes involved (170 - 210 μL of solution) monitoring of the degradation process was carried out using UHPLC and GC–MS. Production of the cell components using stereolithography 3D printing methodologies enabled rapid production of multiple closed BPE cells for BDD particle electrode evaluation. In 600 s a single BDD particle was quantitatively shown to oxidatively remove > 99 % of MB^+ (starting concentration 1×10^{-4} M; equivalent to 3.8 μg) from the solution, with a pseudo first order rate constant of 0.54 min^{-1}. Longer times resulted in complete removal. No intermediate species of the electrochemical breakdown process were detected, within the limits of detection of UHPLC and GC–MS, at all sampling times, $t = 30$ - 900 s. As HPHT synthesis can produce large volumes of BDD particles time efficiently and at a relatively low cost, the data presented indicates the significant potential for HPHT synthesised BDD particles in electrochemical advanced oxidation and related applications. Here large surface area electrodes would be required where it is envisaged the particles could be used in a compacted (porous) form or embedded into a conductive support.

CRediT authorship contribution statement

Anna Dettlaff: Writing – original draft, Visualization, Methodology, Investigation, Formal analysis. **Joshua J. Tully:** Writing – original draft, Visualization, Methodology, Investigation, Formal analysis, Conceptualization. **Georgia Wood:** Conceptualization. **Deep Chauhan:** Investigation. **Ben G. Breeze:** Investigation, Formal analysis. **Lijiang Song:** Investigation, Formal analysis. **Julie V. Macpherson:** Conceptualization, Writing – review & editing, Supervision, Project administration, Funding acquisition.

Declaration of competing interest

The authors declare that they have no known competing financial interests or personal relationships that could have appeared to influence the work reported in this paper.

Data availability

All data used in the preparation of this publication will be made available in an archive (Warwick WRAP).

Acknowledgments

AD thanks Gdańsk University of Technology and the DEC-11/2021/IDUB/II.1/AMERICIUM grant for financial support. JJT, BGB and JVM acknowledge the EPSRC for funding under the Engineered Diamond Technologies program (EP/V056778/1). BGB acknowledges the EPSRC for funding under the WASC programme (EP/V007688/1). We all thank Miss Anjali John and Mr. Dan Houghton (Warwick Chemistry) for running the MB^+ UV–Vis and SEM measurements, respectively. The authors also thank Prof. Dick Crooks (University of Austin, Texas) for

sharing his insights into bipolar electrochemistry.

Supplementary materials

Supplementary information: SI 1: Material Characterization of BDD particles; SI 2: Resistivity calculations; SI 3: Electrochemical degradation of MB; SI 4: UHPLC-MS; SI 5: CV studies of methylene blue using a BDD disc electrode.

Supplementary material associated with this article can be found, in the online version, at doi:10.1016/j.electacta.2024.144035.

References

[1] N. Yang, S. Yu, J.V. MacPherson, Y. Einaga, H. Zhao, G. Zhao, G.M. Swain, X. Jiang, Conductive diamond: synthesis, properties, and electrochemical applications, Chem. Soc. Rev. 48 (2019) 157–204, https://doi.org/10.1039/c7cs00757d.

[2] N. Yang, Novel Aspects of Diamond From Growth to Applications Second Edition, Springer, Siegen, 2019. http://www.springer.com/series/560.

[3] S.J. Cobb, Z.J. Ayres, J.V. Macpherson, Boron doped diamond: a designer electrode material for the twenty-first century, Annu. Rev. Anal. Chem. 11 (2018), https://doi.org/10.1146/annurev-anchem-061417-010107 annurev-anchem-061417-010107.

[4] R.M. Chrenko, Boron, the dominant acceptor in semiconducting diamond, Phys. Rev. B. 7 (1973) 4560–4567, https://doi.org/10.1103/PhysRevB.7.4560.

[5] J.V. Macpherson, A practical guide to using boron doped diamond in electrochemical research, Phys. Chem. Chem. Phys. 17 (2015) 2935–2949, https://doi.org/10.1039/c4cp04022h.

[6] G.F. Wood, C.E. Zvoriste-Walters, M.G. Munday, M.E. Newton, V. Shkirskiy, P. R. Unwin, J.V. Macpherson, High pressure high temperature synthesis of highly boron doped diamond microparticles and porous electrodes for electrochemical applications, Carbon N. Y. 171 (2021) 845–856, https://doi.org/10.1016/j.carbon.2020.09.038.

[7] G.F. Wood, I.M. Terrero Rodríguez, J.J. Tully, S. Chaudhuri, J.V. Macpherson, Electrochemical ozone generation using compacted high pressure high temperature synthesized boron doped diamond microparticle electrodes, J. Electrochem. Soc. 168 (2021) 126514, https://doi.org/10.1149/1945-7111/ac3ff4.

[8] C.A. Martínez-Huitle, M. Panizza, Electrochemical oxidation of organic pollutants for wastewater treatment, Curr. Opin. Electrochem. 11 (2018) 62–71, https://doi.org/10.1016/j.coelec.2018.07.010.

[9] F.C. Moreira, R.A.R. Boaventura, E. Brillas, V.J.P. Vilar, Electrochemical advanced oxidation processes: a review on their application to synthetic and real wastewaters, Appl. Catal. B Environ. 202 (2017) 217–261, https://doi.org/10.1016/j.apcatb.2016.08.037.

[10] S. Garcia-Segura, J. Keller, E. Brillas, J. Radjenovic, Removal of organic contaminants from secondary effluent by anodic oxidation with a boron-doped diamond anode as tertiary treatment, J. Hazard. Mater. 283 (2015) 551–557, https://doi.org/10.1016/j.jhazmat.2014.10.003.

[11] J. Radjenovic, N. Duinslaeger, S.S. Avval, B.P. Chaplin, Facing the Challenge of Poly- And Perfluoroalkyl Substances in Water: is Electrochemical Oxidation the Answer? Environ. Sci. Technol. 54 (2020) 14815–14829, https://doi.org/10.1021/acs.est.0c06212.

[12] C.A. Martínez-Huitle, E. Brillas, Decontamination of wastewaters containing synthetic organic dyes by electrochemical methods: a general review, Appl. Catal. B Environ. 87 (2009) 105–145, https://doi.org/10.1016/j.apcatb.2008.09.017.

[13] S. Alcocer, A. Picos, A.R. Uribe, T. Pérez, J.M. Peralta-Hernández, Comparative study for degradation of industrial dyes by electrochemical advanced oxidation processes with BDD anode in a laboratory stirred tank reactor, Chemosphere 205 (2018) 682–689, https://doi.org/10.1016/j.chemosphere.2018.04.155.

[14] A. Chmayssem, S. Taha, D. Hauchard, Scaled-up electrochemical reactor with a fixed bed three-dimensional cathode for electro-Fenton process: application to the treatment of bisphenol A, Electrochim. Acta. 225 (2017) 435–442, https://doi.org/10.1016/j.electacta.2016.12.183.

[15] R. Zhu, Z. Deng, Y. Wang, K. Zhou, Z. Yu, L. Ma, Q. Wei, A nanoporous diamond particle microelectrode and its surface modification, Electrochim. Acta. 430 (2022) 141015, https://doi.org/10.1016/j.electacta.2022.141015.

[16] T. Ando, K. Asai, J. Macpherson, Y. Einaga, T. Fukuma, Y. Takahashi, Nanoscale reactivity mapping of a single-crystal boron-doped diamond particle, Anal. Chem. 93 (2021) 5831–5838, https://doi.org/10.1021/acs.analchem.1c00053.

[17] S.E. Fosdick, K.N. Knust, K. Scida, R.M. Crooks, Bipolar electrochemistry, Angew. Chem. - Int. Ed. 52 (2013) 10438–10456, https://doi.org/10.1002/anie.201300947.

[18] J.P. Guerrette, S.M. Oja, B. Zhang, Coupled electrochemical reactions at bipolar microelectrodes and nanoelectrodes, Anal. Chem. 84 (2012) 1609–1616, https://doi.org/10.1021/ac2028672.

[19] J.T. Cox, J.P. Guerrette, B. Zhang, Steady-state voltammetry of a microelectrode in a closed bipolar cell, Anal. Chem. 84 (2012) 8797–8804, https://doi.org/10.1021/ac302219p.

[20] E. Laborda, A. Molina, Coupled electron transfer reactions in closed bipolar cells: the impact of asymmetric mass transport, Curr. Opin. Electrochem. 39 (2023) 101287, https://doi.org/10.1016/j.coelec.2023.101287.

[21] D. Plana, G. Shul, M.J. Stephenson, R.A.W. Dryfe, The voltammetric response of bipolar cells: mechanistic investigations of electroless deposition, Electrochem. Commun. 11 (2009) 61–64, https://doi.org/10.1016/j.elecom.2008.10.034.

[22] W. Xu, K. Fu, C. Ma, P.W. Bohn, Closed bipolar electrode-enabled dual-cell electrochromic detectors for chemical sensing, Analyst 141 (2016) 6018–6024, https://doi.org/10.1039/C6AN01415A.

[23] C. Oh, B. Park, V. Sundaresan, J.L. Schaefer, P.W. Bohn, Closed bipolar electrode-enabled electrochromic sensing of multiple metabolites in whole blood, ACS Sensors 8 (2023) 270–279, https://doi.org/10.1021/acssensors.2c02140.

[24] N.L. Walker, J.E. Dick, Leakless, bipolar reference electrodes: fabrication, performance, and miniaturization, Anal. Chem. 93 (2021) 10065–10074, https://doi.org/10.1021/acs.analchem.1c00675.

[25] N.L. Walker, J.E. Dick, On the mechanism of the bipolar reference electrode, Analyst 148 (2023) 2149–2158, https://doi.org/10.1039/D3AN00107E.

[26] S. Takano, K.Y. Inoue, M. Ikegawa, Y. Takahashi, K. Ino, H. Shiku, T. Matsue, Liquid-junction-free system for substitutional stripping voltammetry using a closed bipolar electrode system, Electrochem. Commun. 66 (2016) 34–37, https://doi.org/10.1016/j.elecom.2016.02.014.

[27] J.J. Tully, G.N. Meloni, A scientist's guide to buying a 3D printer: how to choose the right printer for your laboratory, Anal. Chem. 92 (2020) 14853–14860, https://doi.org/10.1021/acs.analchem.0c03299.

[28] W.L. Wang, M.C. Polo, G. Sánchez, J. Cifre, J. Esteve, Internal stress and strain in heavily boron-doped diamond films grown by microwave plasma and hot filament chemical vapor deposition, J. Appl. Phys. 80 (1996) 1846–1850, https://doi.org/10.1063/1.362996.

[29] A.F. Azevedo, R.C. Mendes de Barros, S.H.P. Serrano, N.G. Ferreira, SEM and Raman analysis of boron-doped diamond coating on spherical textured substrates, Surf. Coatings Technol. 200 (2006) 5973–5977, https://doi.org/10.1016/j.surfcoat.2005.09.012.

[30] D. Kumar, M. Chandran, M.S. Ramachandra Rao, Effect of boron doping on first-order Raman scattering in superconducting boron doped diamond films, Appl. Phys. Lett. (2017) 110, https://doi.org/10.1063/1.4982591.

[31] Z. Liu, S. Baluchová, A.F. Sartori, Z. Li, Y. Gonzalez-Garcia, M. Schreck, J. G. Buijnsters, Heavily boron-doped diamond grown on scalable heteroepitaxial quasi-substrates: a promising single crystal material for electrochemical sensing applications, Carbon N. Y. 201 (2023) 1229–1240, https://doi.org/10.1016/j.carbon.2022.10.023.

[32] G. Wosiak, M.C. Silva, J. da Silva, E.B. Carneiro-Neto, M.C. Lopes, E. Pereira, Evaluation of interfacial pH change during water splitting at pulsed regime using finite element method, Int. J. Hydrogen Energy. 46 (2021) 17644–17652, https://doi.org/10.1016/j.ijhydene.2021.02.195.

[33] D. Becker, K. Jüttner, The impedance of fast charge transfer reactions on boron doped diamond electrodes, Electrochim. Acta. 49 (2003) 29–39, https://doi.org/10.1016/j.electacta.2003.04.003.

[34] D.A. Armstrong, R.E. Huie, W.H. Koppenol, S.V. Lymar, G. Merényi, P. Neta, B. Ruscic, D.M. Stanbury, S. Steenken, P. Wardman, Standard Electrode Potentials Involving Radicals in Aqueous Solution: Inorganic Radicals, 2016.

[35] A.J. Bard, L.R. Faulkner, Electrochemical Methods - Fundamentals and Applications, 2nd ed., Wiley, 2001.

[36] J.A. Caram, J.F.M. Suárez, A.M. Gennaro, M.V. Miríffico, Electrochemical behaviour of methylene blue in non-aqueous solvents, Electrochim. Acta 164 (2015) 353–363, https://doi.org/10.1016/j.electacta.2015.01.196.

[37] A. Aleboyeh, M.B. Kasiri, H. Aleboyeh, Influence of dyeing auxiliaries on AB74 dye degradation by UV/H_2O_2 process, J. Environ. Manage. 113 (2012) 426–431, https://doi.org/10.1016/j.jenvman.2012.10.008.

[38] S. Hisaindee, M.A. Meetani, M.A. Rauf, Application of LC-MS to the analysis of advanced oxidation process (AOP) degradation of dye products and reaction mechanisms, TrAC - Trends Anal. Chem. 49 (2013) 31–44, https://doi.org/10.1016/j.trac.2013.03.011.

[39] C. Comninellis, G. Chen, Electrochemistry For the Environment, Springer, London, 2010.

[40] P. Cañizares, B. Louhichi, A. Gadri, B. Nasr, R. Paz, M.A. Rodrigo, C. Saez, Electrochemical treatment of the pollutants generated in an ink-manufacturing process, J. Hazard. Mater. 146 (2007) 552–557, https://doi.org/10.1016/j.jhazmat.2007.04.085.

[41] N. Martin, Y. Leprince-wang, HPLC-MS and UV – visible coupled analysis of methylene blue photodegradation by hydrothermally grown ZnO nanowires, Phys. Status Solidi. 218 (2021) 2100532, https://doi.org/10.1002/pssa.202100532.

[42] X. Teng, J. Li, Z. Wang, Z. Wei, C. Chen, K. Du, C. Zhao, G. Yang, Y. Li, Performance and mechanism of methylene blue degradation by an electrochemical process, RSC Adv. 10 (2020) 24712–24720, https://doi.org/10.1039/d0ra03963b.

[43] E. Barou, M. Bouvet, O. Heintz, R. Meunier-Prest, Electrochemistry of methylene blue at an alkanethiol modified electrode, Electrochim. Acta 75 (2012) 387–392, https://doi.org/10.1016/j.electacta.2012.05.017.

[44] T. Moazzenzade, X. Yang, L. Walterbos, J. Huskens, C. Renault, S.G. Lemay, Self-Induced convection at microelectrodes via electroosmosis and its influence on impact electrochemistry, J. Am. Chem. Soc. 142 (2020) 17908–17912, https://doi.org/10.1021/jacs.0c08450.